Cathodic NH_4^+ Leaching of Nitrogen Impurities in CoMo Thin-film Electrodes in Aqueous Acidic Solutions

Weilai Yu[a] , Pakpoom Buabthong[b], Carlos G. Read[a], Nathan F. Dalleska[c], Nathan S. Lewis[a], Hans-Joachim Lewerenz[b], Harry B. Gray[a*] and Katharina Brinkert[a,d*]

a. Division of Chemistry and Chemical Engineering, California Institute of Technology, 1200 E California Blvd., Pasadena, CA 91125, USA.

b. Division of Engineering and Applied Science, California Institute of Technology, 1200 E California Blvd., Pasadena, CA 91125, USA.

c. Environmental Analysis Center, Division of Geology and Planetary Science, California Institute of Technology, 1200 E California Blvd., Pasadena, CA 91125, USA.

d. Department of Chemistry, University of Warwick, Gibbet Hill Road, Coventry, CV4 7AL, UK.

Email: hbgray@caltech.edu; katharina.brinkert@warwick.ac.uk

Abstract

Electrocatalytic reduction of dinitrogen (N_2) to ammonium (NH_4^+) in acidic aqueous solutions was investigated at ambient temperature and pressure using a cobalt-molybdenum (CoMo) thin-film electrode prepared by magnetron reactive sputtering. Increased concentrations of ammonium ions (NH_4^+) were consistently detected in the electrolyte using ion chromatography (IC) after constant-potential electrolysis at various potentials (≤-0.29 V *vs.* RHE). Using a newly developed analytical method based on ammonia derivatization, performing the experiments with $^{15}N_2$-labelled gas led however to the detection of increased $^{14}NH_4^+$ concentrations instead of $^{15}NH_4^+$. X-ray photoelectron spectroscopic (XPS) analysis of the electrode surface revealed the presence of Mo≡N and Mo-NH_x species. Several contamination sources were identified that led to substantial increases in the concentration of ammonium ions, including $^{15}NH_3$ impurities in $^{15}N_2$ gas. The observed ammonium concentrations can be consistently ascribed to leaching of nitrogen (^{14}N) impurities incorporated in the CoMo film during the sputtering process. Researchers in the field are therefore urged to adopt extended protocols to identify and eliminate sources of ammonia contamination and to very carefully monitor the ammonium concentrations in each experimental step.

Introduction

The discovery of ammonia (NH_3) synthesis, a milestone in the history of the chemical industry, has greatly enhanced global agriculture. Ammonia is the second-largest chemical produced worldwide, with 140 million tons manufactured annually via the Haber-Bosch process.[1] The process requires high-purity streams of $N_2(g)$ and $H_2(g)$, as well as high temperatures (400-500 °C) and high pressures (200-300 atm). Notably, ammonia synthesis consumes ~ 1% of the energy used on our planet.

Mild methods to break the N-N triple bond represent a major opportunity for catalyst development.[2–5] Electrochemically based nitrogen reduction could use renewable solar and wind electricity to drive reactions at ambient temperature and pressure,[5–10] thereby providing a sustainable technology for widespread production of ammonia for fertilizer and fuels.

Although the standard potential of reduction of dinitrogen to ammonia is similar to the standard potential of the hydrogen-evolution reaction (HER), the latter is kinetically favored:[11]

$$N_2(g) + 6H^+(aq) + 6e^- \rightarrow 2NH_3(aq) \qquad E° = +0.092 \text{ V } \textit{vs.} \text{ RHE} \qquad (1)$$

$$2H^+(aq) + 2e^- \rightarrow H_2(g) \qquad E° = 0.00 \text{ V } \textit{vs.} \text{ RHE} \qquad (2)$$

where RHE is the potential of the reversible hydrogen electrode. The high dissociation enthalpy (942 kJ mol^{-1}) of the N_2 triple bond and the required multiple proton-coupled electron transfer (PCET) steps lead to high overpotentials for direct conversion to NH_3. The high N_2 activation barrier compared to that of the HER, together with the low solubility of N_2 in H_2O, present major selectivity challenges for electrochemical N_2 reduction.

Among pure metals, Ru and Os are the best catalysts for gas-phase ammonia production from H_2 and N_2,[12] accomplishing the trade-off between a high nitrogen adsorption energy on the surface and a low activation energy for the dissociative step. In the quest for robust and active earth-abundant catalytic materials, mixed-metal systems such as the ternary metal nitride Co_3Mo_3N have shown promise for gas-phase ammonia production.[13,14] These catalysts are believed to fix nitrogen via the Mars-van Krevelen mechanism,[15,16] in which activated surface nitride participates in the reaction.[17] A theoretical analysis has indicated that MoN might catalyze electrochemical nitrogen reduction (NRR) under ambient conditions.[18] Although CoMo bimetallic nanoparticles exhibit similar gas-phase ammonia-production activities as those of Ru nanoparticles,[19] CoMo has not hitherto been explored extensively for electrochemical NRR under ambient conditions.

In addition to the considerations involving electrocatalyst materials, increasing emphasis has been placed on the design and execution of experiments for investigations of the electrochemical reduction of N_2 to NH_3.[20–23] Many contamination sources have been identified that can give rise to increased ammonia concentrations in electrolytes and thereby confound formulation of robust conclusions concerning the true efficacy of the electrocatalyst. Consequently, $^{15}N_2$ isotope-labelled electrochemical experiments are crucial to confirm the putative activity for electrochemical N_2 reduction.[23] In addition, analytical methods need to be user-friendly and enable isotope-selective quantification of μM concentrations of ammonia.[21,24]

Herein, we present a comprehensive investigation of the electrochemical activity of CoMo thin-film electrodes prepared by magnetron sputtering. To quantify $^{14}N/^{15}N$-labelled ammonium ions at μM concentration levels with isotope selectivity, we used an analytical method based on ammonia

derivatization with dansyl chloride. Moreover, the electrode surfaces were characterized before and after electrochemical experiments using scanning-electron microscopy (SEM), atomic-force microscopy (AFM) and X-ray photoelectron spectroscopy (XPS) techniques. Despite the generally preserved surface morphology and evidence for the presence of Mo≡N and Mo-NH_x species on the electrode surface by XPS, we were not able to confirm electrocatalytic reduction of dinitrogen through $^{15}N_2$ labelling experiments. On the contrary, the observed increases in ammonium concentrations can be ascribed to leaching under cathodic conditions of nitrogen impurities from the sputtered CoMo thin-film. Based on the present results and identified $^{14}NH_4^+$ contamination sources, we conclude that additional protocols must be adopted before a robust claim can be sustained that NH_3 is a product of electrochemical N_2 reduction.[20,22,23]

Results and Discussion

Electrochemistry and ammonium yields (n^+-Si/Ti/CoMo electrodes) using $^{14}N_2$ gas. A CoMo thin-film was deposited using reactive magnetron sputtering onto a degenerately-doped n-type Si substrate that had been coated with a Ti adhesion layer. This deposition technique offers the advantage of close proximity and versatile composition-tuning between the two different elements. A pure Ar atmosphere (flow rate = 20 sccm and pressure = 5 mTorr) was used during the deposition process. Cross-sectional and high-resolution TEM images of the n^+-Si/Ti/CoMo electrode are shown in Figure S1.

Initial electrochemical studies of CoMo electrodes revealed stable current densities for 1 h under a constant N_2(g) purge in a three-electrode cell with static electrolytes of 50 mM sulfuric acid, with either water or ethanol as solvent (Figure S2). At a potential of -0.54 V *vs.* RHE, a cathodic current density of ~ 7.4 mA cm^{-2} was observed in aqueous H_2SO_4, whereas the cathodic current density in the ethanolic electrolyte was ~ 0.8 mA cm^{-2}. The much lower current density in the ethanolic electrolyte was due to suppression of the competing HER. As shown in Figure 1a, the highest ammonia production rate (0.19 ± 0.02 nmol·cm^{-2}·s^{-1}) was obseved in aqueous H_2SO_4 after 1 h, whereas the rate was slightly lower after 20 min of electrolysis (0.16 ± 0.01 nmol·cm^{-2}·s^{-1}). After 12 h at constant potential, the ammonium production rate decreased by about 80% to 0.03 ± 0.01 nmol·cm^{-2}·s^{-1}. Notably, the total ammonium yield after 12 h operation (1.3 ± 0.43 µmol·cm^{-2}) was only ~2.3 times higher than the total yield after 1 h operation (0.69 ± 0.09 µmol cm^{-2}) (Figure 1c). Faradaic efficiencies in the aqueous system were ~ 0.6 ± 0.01% assuming that electrochemical NRR occurred. Owing to suppression of the HER, higher Faradaic efficiencies (FEs) were observed in the ethanolic electrolyte, with values of ~ 3.3 ± 0.3% after 20 min and ~ 1.3 ± 0.2% after

1 h of operation.

Ion chromatography (IC) was used to quantify the ammonium concentrations in the electrolytes after each experiment. Relative to colorimetric methods,[25] IC has substantially better accuracy and lower limits of detection (Figure S3). To better quantify ammonium yields originating from the electrochemical process and to exclude ammonia contamination from various sources, control experiments were performed using the CoMo electrode, and the results were compared to those from analogue experiments using Co, Mo, NiMo and FeMo films, respectively, deposited on the n^+-Si/Ti substrate (Table S1). First, a background ammonium concentration of 1.1 μM was determined in the 50 mM H_2SO_4 electrolyte. After leaving the CoMo electrode in the electrolyte at the open-circuit potential (E_{oc} ~ 0.03 V *vs.* RHE) for 20 min, the detected ammonium concentrations ranged from 0.9-2.5 μM. After 12 h at E_{oc} in 50 mM H_2SO_4(aq), the background ammonia concentration produced by the n^+-Si/Ti/CoMo electrode doubled from 1.4 to 2.8 μM. Furthermore, a gas bubbler containing 50 mM H_2SO_4(aq) was used to remove potential ammonia impurities in the purged N_2 gas. After purging the electrochemical cell for > 60 min, no increase in ammonium concentration was observed, thereby confirming the absence of ammonia impurities originating from purging with Ar or N_2(g). A slightly higher ammonium concentration was observed (2.0-2.45 μM) when the solvent was switched from water to ethanol, suggesting that the background depended on the electrolyte system, consistent with the different solubility of ammonium in different solvents. Control experiments clearly must be performed so that correction for any background ammonium concentration can be made when quantifying the amount of ammonium produced by electrocatalysis.

Table 1 contains a comparison of various sputtered thin-film electrodes under potential control for 20 min

at -0.54 V *vs.* RHE. The highest yields of ammonium were observed for CoMo electrodes in 50 mM H_2SO_4(aq). Switching electrolyte anions from SO_4^{2-} to Cl^- or ClO_4^- led to lower ammonium yields after 20 min under potential control. Under nominally identical conditions, elementary Co and Mo electrodes led to much lower ammonium yields, along with lower current densities, than were observed for CoMo. Morevoer, substituting Ni or Fe for Co also decreased the resulting ammonium yield (Table 1). The potential (E) dependence of the ammonium yields in aqueous H_2SO_4 was determined for a CoMo electrode over 20-min periods (Figure 1b). The highest yield (225.2 ± 23.6 nmol·cm^{-2}) was observed after 20 min for E = -1.29 V *vs.* RHE, whereas the yield decreased to 145.2 ± 26.7 nmol·cm^{-2} for E = -0.79 V and increased to 192.9 ± 11.7 nmol·cm^{-2} for E = -0.54 V, before decreasing again to 95.8 ± 31.4 nmol·cm^{-2} for E = -0.29 V.

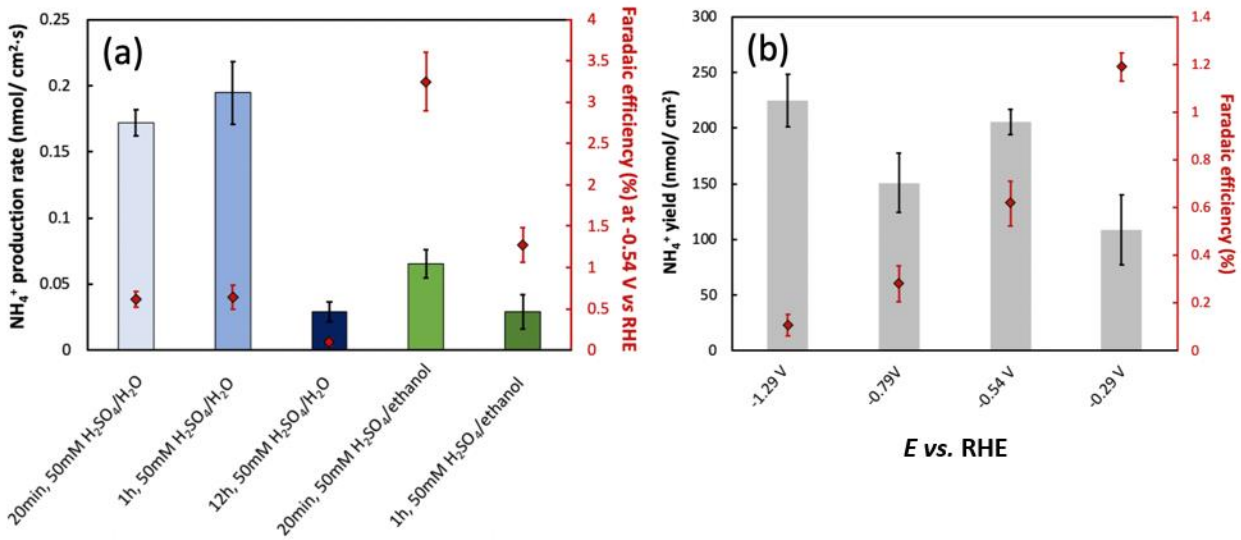

Figure 1. (a) NH_4^+-production rates in aqueous and ethanolic 50 mM H_2SO_4 as a function of electrolysis time. The secondary y-axis (data are filled diamonds) shows Faradaic efficiencies of the n^+-Si/Ti/CoMo

electrodes for the respective electrochemical conditions, assuming that electrochemical NRR occurs. (b) NH_4^+-production yields of 20 min tests in aqueous 50 mM H_2SO_4 at different potentials. The NH_4^+-production yields and rates were corrected for background NH_4^+ values obtained with samples held under open-circuit conditions in the same electrolyte for the same time period (compare Table S1). Unless indicated otherwise, the potential was -0.54 V *vs.* RHE. The error bars represent standard deviations from three independent electrochemical tests with fresh electrodes for each condition.

Table 1. Comparison of NH_4^+ yields after 20 min constant potential electrolyses with different electrodes. Calculated NH_4^+ yields were corrected against background NH_4^+ values obtained with the sample under open-circuit conditions in the same electrolyte for the same time period (Table S1). The potential was -0.54 V *vs.* RHE, and the electrolyte was 50 mM aqueous H_2SO_4 (if not indicated otherwise).

Sample	**NH_4^+ yield (nmol cm^{-2})**	**c(NH_4^+) (μM cm^{-2})**	**J (mA cm^{-2})**	**FE (%)**
CoMo	193	9.6	7.36	0.63
CoMo, 50mM HCl	47	2.3	4.05	0.28
CoMo, 50mM $HClO_4$	4.8	0.2	4.17	0.03
Co	20	1.0	2.13	0.22
Mo	4	0.2	5.54	0.02
FeMo	0	0	4.29	0
NiMo	34	1.7	7.13	0.12

Surface morphology and topography. Atomic-force microscopy (AFM) and high-resolution scanning-electron microscopy (HRSEM) were used to probe changes in surface morphology of the CoMo electrode before and after electrochemical experiments, respectively. As evident from Figure 2a-c, an as-prepared

CoMo thin-film exhibited a nano-particulate surface morphology that was largely preserved after the electrode was held for 1 to 12 h at -0.54 V *vs.* RHE. Based on the AFM images (Figure 2d-f), the initial surface roughness for an as-prepared CoMo thin-film was ~1 nm. After 1 h at -0.54 V *vs.* RHE, the electrode surface slightly roughened (roughness increased from 1 to 3 nm), and displayed higher film porosity with larger average particle size. Changes in CoMo surface morphology were even more evident after 12 h under potential control, with small particles (~3 nm) distributed among larger particles (~55 nm).

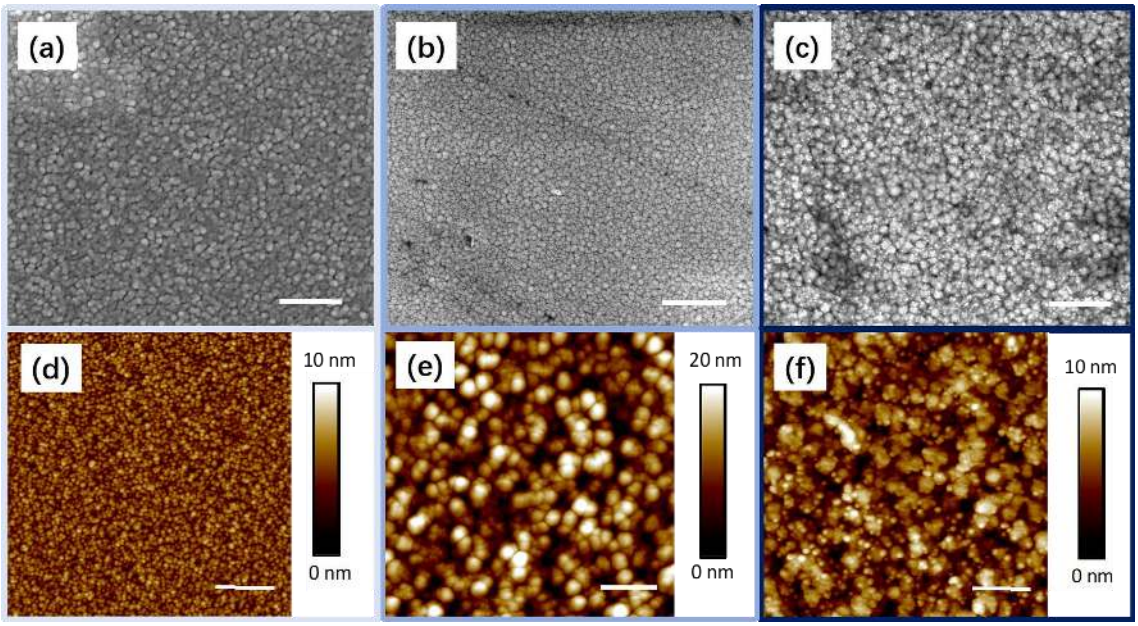

Figure 2. (a-c) HRSEM images of n^+-Si/Ti/CoMo surfaces: samples (a) before electrochemical testing; (b) after 1 h; and (c) after 12 h in aqueous 50 mM H_2SO_4 at E = -0.54 V *vs.* RHE (500 nm scale bars). (d-f) AFM images of samples (a)-(c), 200 nm scale bars.

Surface composition analysis by XPS. To assess compositional changes of the surface, X-ray photoelectron spectroscopy (XPS) was performed before electrochemical testing (Figure 3, top), as well as after applying E = -0.54 V *vs.* RHE to a CoMo electrode in aqueous electrolyte for 20 min (center) or 12 h (bottom). Peak assignments are based on previous reports and peak positions used in the analysis are listed in Table S2.[26–28] Before electrochemical tests, the surface of an as-prepared CoMo thin-film was enriched in Mo^0 and Co^0 (combined with various oxide species). The dominant peak in the Co spectrum can be assigned to Co^0 with 13-22% surface oxides in the form of Co^{2+}, Co^{3+}, and Co-OH moieties, likely resulting from exposure to moisture and/or air (Figure 3a).[26–28] Based on the Mo 3d spectrum, $Mo^{2+/3+}$, $Mo^{3+/4+}$ and two Mo^{6+} species were present (Figure 3b).[26–28]

Deconvolution of the N 1s spectrum was performed after accounting for partially overlapping Mo $3p^{3/2}$ features (Figure 3c). The N 1s spectrum of an as-prepared CoMo sample was partially obscured by a dominant Mo 3p peak attributable to MoO_3. After constant potential electrolysis at E = -0.54 V *vs.* RHE for 20 min or 12 h, only Co^0 remained on the electrode surface (multiple CoO_x peaks disappeared, Figure 3 and Figure S4). Moreover, the amount of surface MoO_x was substantially reduced and the surface Mo^0 coverage increased to ~ 66% of the total Mo signal. As seen in Figure 3b, the Mo^{6+} species (yellow) associated with surface MoO_3 disappeared and the Mo^{6+} peak (red) at lower binding energies remained, with the latter feature due to a Mo^{6+} nitride (Mo≡N). The Mo≡N signal first increased from 4% of the total Mo signal (as-prepared) to ~ 8% after 20-min under potential control and then to ~14% of the total Mo signal after 12 h under potential control. After electrochemical testing, removal of surface MoO_3 was apparent from the N 1s spectrum, as were distinctive features attributable to Mo-NH_3^+, Mo-NH_2 and

Mo≡N species (high to low B.E., respectively).[26] After 10-min immersion at open circuit in 10 mM KOH(aq), the intensity of the Mo-NH_2 feature increased, along with disappearance of Mo-NH_3^+ on the electrode surface (Figure S5). These findings suggest deprotonation of surface-adsorbed ammonium species in aqueous alkaline solutions. The collective XPS data confirm that adsorbed NH_x species were present on electrochemically evaluated CoMo electrode surfaces.

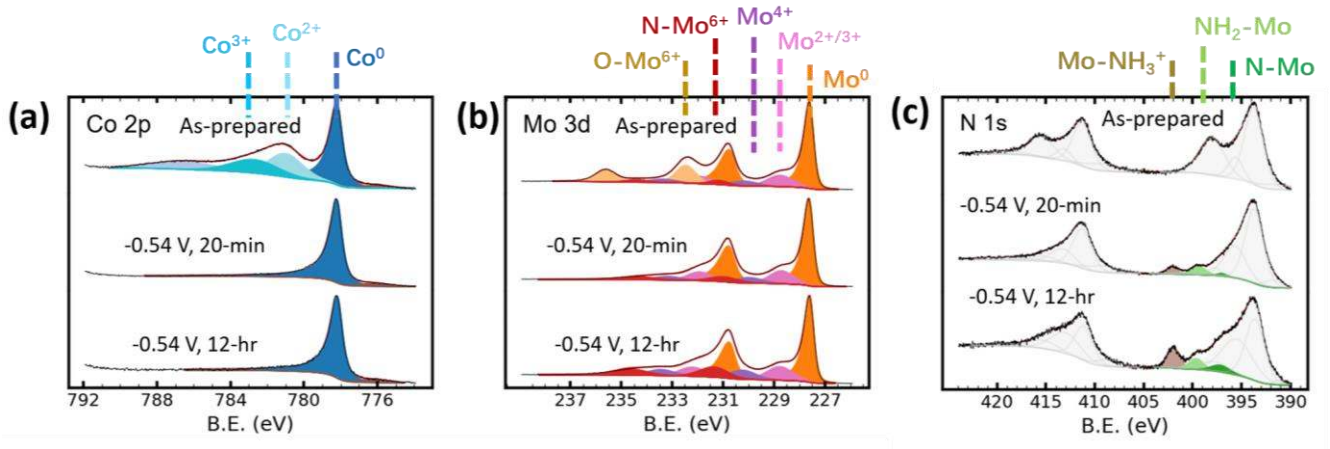

Figure 3. X-ray photoelectron spectra of the CoMo surface prior to electrocatalysis (top); after 20 min under potential control (center); and after 12 h (bottom) in aqueous 50 mM H_2SO_4 at a potential of -0.54 V *vs.* RHE. (a) Co 2p core levels; (b) Mo 3d core levels and (c) N 1s core levels. B.E. is the binding energy.

Electrochemical experiments with $^{15}N_2$. Experiments with $^{15}N_2$ gas were performed to determine definitively whether the detected ammonia was generated by electrochemical reduction of nitrogen catalysed by Co-Mo. The low-μM $^{15}NH_4^+$ concentrations were difficult to quantify with isotope-selectivity, either by NMR or by ion chromatography coupled mass spectrometry (IC-MS). This issue was addressed by using a new analytical method that allowed simultaneous quantification of $^{14}NH_4^+$ and $^{15}NH_4^+$

concentrations at sub-μM level.[29] In this procedure, dansyl chloride was used to derivatize ammonia at room temperature and optimal pH (Equation S1), with the derivatized products subsequently analyzed by ultrahigh-performance liquid chromatography coupled mass spectrometry (UPLC-MS). The molecular derivates of $^{14}NH_4^+/^{15}NH_4^+$ ions were isotopically distinguished by their different masses and quantified based on their respective peak areas.

An acid trap was required to purify $^{15}N_2$ gas (Sigma Aldrich, No. 364584) before electrochemical experiments. After purging for 90 min, the gas-scrubber solution (~5 mL of 50 mM H_2SO_4(aq)) contained substantially increased concentrations of $^{14}NH_4^+$ (18.5 μM) and $^{15}NH_4^+$ ions (33 μM), indicating that $^{14}NH_3$ and $^{15}NH_3$ impurities were present in the $^{15}N_2$ gas (Figure 4).[30] An acid trap (Figure S6) was thus required to first purify $^{15}N_2$ gas prior to any electrochemical experiments. Based on the results in Figure 1, isotope-labelled $^{15}N_2$ experiments were repeated for all potentials previously used with CoMo electrodes. To exclude contamination with ammonia, electrolyte samples were examined after three different experimental steps: (a) after the electrolyte was transferred into the cell; (b) after Ar and $^{15}N_2$ purging and before the electrode was placed in the cell for testing; and (c) after performing 20-min electrolyses. Table 2 provides a comparison of the $^{15}NH_4^+$ concentrations observed at different electrode potentials. Despite the presence of ammonia impurities in $^{15}N_2$ gas, no increases in $^{15}NH_4^+$ concentrations were observed in the setup with an acid trap for entry 1-5 after $^{15}N_2$ purging. Hence the $^{15}NH_3$ impurities were removed from $^{15}N_2$ gas prior to purging the electrolyte.

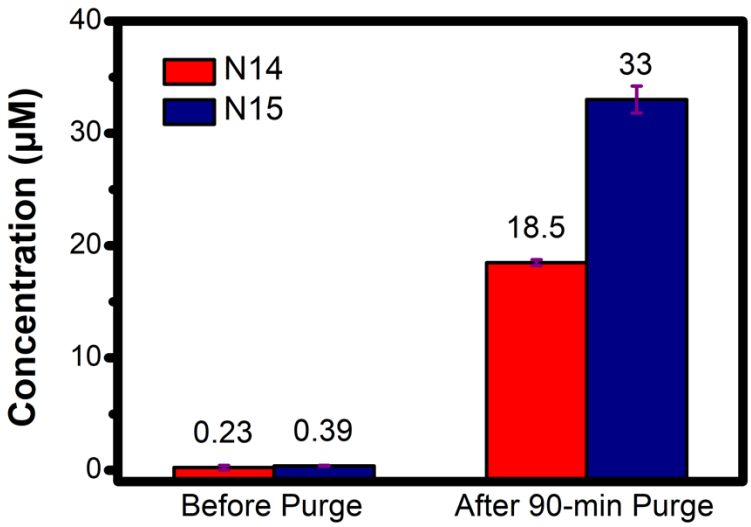

Figure 4. Comparison of $^{14}NH_4^+/^{15}NH_4^+$ concentrations in the gas scrubber solution (~5 mL of 50 mM H_2SO_4) before and after, respectively, purging $^{15}N_2$ gas for 90 min. Concentrations were determined by ammonia derivatization with dansyl chloride followed by UPLC-MS analysis.

Isotope-labelling experiments were repeated at different potentials and did not yield any detectable increases in the concentrations of $^{15}NH_4^+$. However, substantial increases in $^{14}NH_4^+$ concentrations were consistently observed for all conditions (Table 2). As shown in Figure 5 and Table S3, normalized increases in $^{14}NH_4^+$ concentrations after electrolyses with $^{15}N_2$ were comparable to those obtained in electrolyses with $^{14}N_2$ gas. Within the same time period (20 min), $^{14}NH_4^+$ concentrations also increased as the electrode potential became more negative. This trend corresponds to higher cathodic current densities at more negative potentials, a large portion of which directly affects the HER (Figure S7).

Table 2. Comparison of $^{15}NH_4^+$ concentrations obtained from experiments at three different steps for five electrochemical tests (20 min) at various potentials using $^{15}N_2$ gas. Concentrations were determined using dansylation followed by UPLC-MS analyses. Three UPLC-MS measurements were performed for each sample.

Entry	*E* (V *vs.* RHE)	Before purge[a] (μM)	After purge[b] (μM)	After 20 min at constant *E*[c] (μM)
1	-0.29	0.49 ± 0.10	0.45 ± 0.06	0.65 ± 0.3
2	-0.54	0.74 ± 0.08	1.0 ± 0.3	1.0 ± 0.5
3	-0.54[d]	0.79 ± 0.02	0.79 ± 0.08	0.73 ± 0.08
4	-0.79	0.41 ± 0.09	1.1 ± 0.2	1.5 ± 0.6
5	-1.29	0.47 ± 0.1	0.49 ± 0.09	1.2 ± 0.7

[a]Electrolytes were sampled immediately after filling the cell; [b]electrolytes were sampled after Ar/$^{15}N_2$ purging with reference and counter electrodes in the cell; [c]electrolytes were sampled after putting electrodes into each cell and testing for 20 min; [d] electrolyses with *E* = -0.54 V *vs.* RHE were repeated twice.

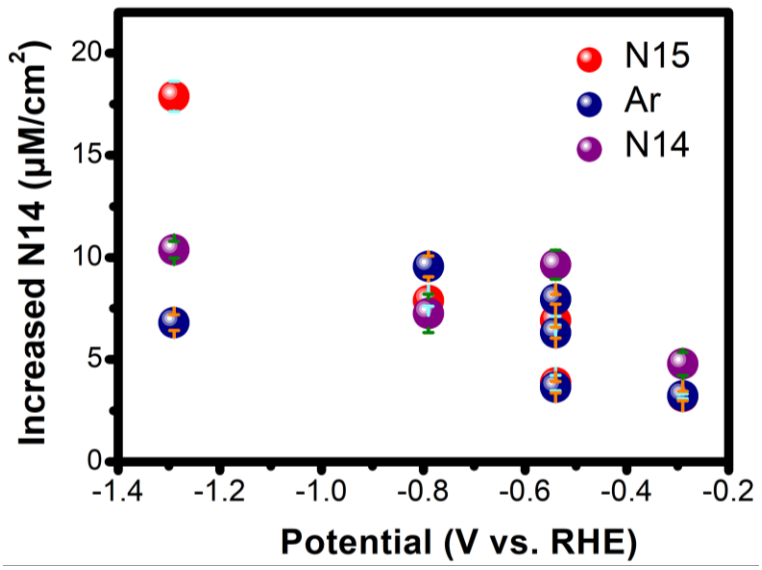

Figure 5. Comparison of increased $^{14}NH_4^+$ concentrations (normalized by electrode areas) for 20-min electrochemical experiments using CoMo electrodes at -0.54 V *vs.* RHE, purging with $^{15}N_2/Ar/^{14}N_2$ gases. The electrolytes obtained from $Ar/^{15}N_2$-purging experiments (red and blue) were analyzed by the dansyl chloride derivatization/UPLC-MS method; each error bar is based on three UPLC-MS measurements of the same sample. The $^{14}N_2$ data points (purple) are the same as those in Figure 1; each error bar is based on three independent experiments in which the electrolytes were analyzed by IC.

Ammonia contamination sources. Based on the present results, the increased ammonium concentrations detected after electrochemical experiments (Figure 1) likely do not originate from electrochemical reduction of N_2. Interestingly, compared to operation at E_{oc} (Table S1), substantial ammonium concentrations were only observed for CoMo electrodes held under cathodic conditions. During electrochemical experiments, the epoxy and the CoMo thin-film were the only two components in direct contact with electrolyte. All electrodes were made using the same epoxy (Loctite 9460), so the effect of

ammonia contamination from that potential source likely is limited, although most chemically resistant, two-component epoxies contain hardeners based on amines. The ammonia contamination from epoxy can be neglected for short-term experiments, but could impact the ammonia background concentration in electrolyses over longer time periods. We therefore conclude that increased amounts of $^{14}NH_4^+$ in the electrolyte were derived from the CoMo electrodes. Nitrogen impurities can be incorporated in CoMo thin-films during the sputtering process, even in an Ar atmosphere. Unlike the nitride-decomposition mechanism reported previously, nitrogen impurities likely originate from Ar flow gas, sputtering targets or the deposition chamber.[31–33]

To support the above claim, experiments were performed using CoMo electrodes under an Ar purge. Notably, increased amounts of $^{14}NH_4^+$ were consistently observed after 20-min electrolyses at four different potentials (Figure 5). Moreover, these increased $^{14}NH_4^+$ concentrations were comparable to those observed in electrolyses performed with $^{14}N_2/^{15}N_2$ (Table S3). After various electrolyses under Ar purging, XPS analyses revealed Mo≡N and NH_x species at CoMo electrode surfaces similar to those evaluated under $^{14}N_2/^{15}N_2$ purging (Figure 6 and Figure S8-9). These observations collectively indicate that the N species identified at these electrode surfaces were not derived from the purged N_2 gas. To exclude the formation of ammonia via reduction of nitrate (NO_3^-) or nitrite (NO_2^-) ions, the concentrations of both ions in the electrolyte at different experimental stages were measured using IC. Additional results with relevant discussion are available in the SI (Table S4). μM-levels of NO_3^- ions were observed in all electrolyte samples, but NO_2^- was below the detection limit. Using chemiluminescence analysis, negligible NO(g) levels were found in the Ar and $N_2{}^{14}$(g) gas cylinders, whereas the NO_2(g) concentrations were

lower than in the laboratory air. An additional experiment was performed by holding the CoMo electrode for 20 min at -0.54 V *vs.* RHE in 50 mM H_2SO_4(aq) that additionally contained 40.6 µM of pre-existing NO_3^- ions, with no gas purging. The nitrate concentration did not decrease, indicating negliglble nitrate reduction at the CoMo surface.

Furthermore, prolonged storage (10 days) of sampled electrolytes in polypropylene vials (Thermo Scientific C4000-11) led to substantial increases in ammonium concentrations (Table S5).

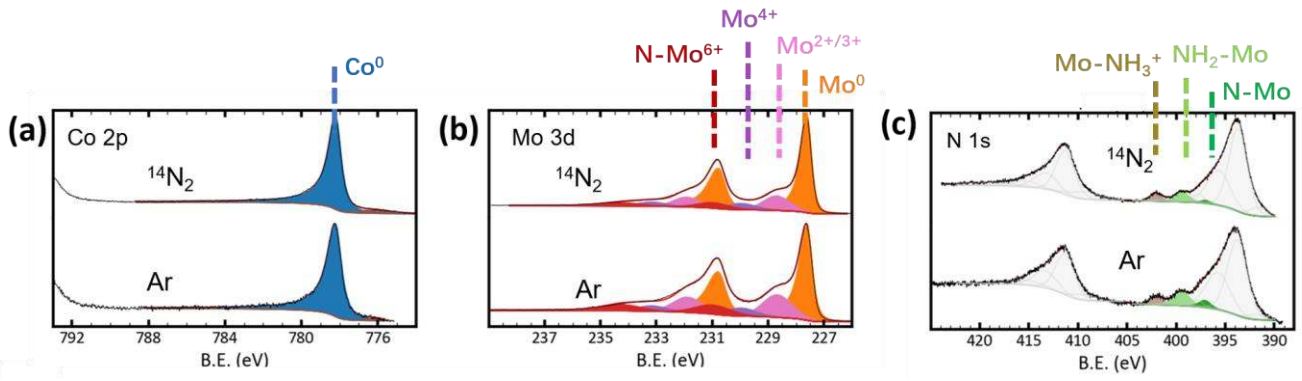

Figure 6. Comparison of X-ray photoelectron spectra of (a) Co 2p, (b) Mo 3d and (c) N 1s for CoMo electrodes tested at -0.54 V *vs.* RHE for 20 min in 50 mM H_2SO_4(aq) under $^{14}N_2$ and Ar purging.

The increases in observed ammonium concentrations after various electrolyses were not dependent on the purge N_2 gas because the increases were produced from the electrode itself under cathodic conditions. The amounts of these incorporated nitrogen impurities depended on the deposited thin-film materials (Table 1). The highest amounts of N impurities were observed for the bimetallic (CoMo) system, consistent with favorable N adsorption/desorption energies in the gas phase.[12] The leaching kinetics of N impurities are

likely regulated by anions in the electrolyte, as demonstrated by different ammonium concentrations observed after tests in 50 mM $HCl/HClO_4$(aq). The presence of self-containing N leaching is also supported by a series of previous observations: (a) the slightly higher porosity of the CoMo thin-film after electrochemical tests; (b) a non-linear increases in total ammonia yields over prolonged testing (12 h), likely due to a plateau effect of N leaching from the electrode; and (c) XPS evidence of surface Mo≡N and NH_x species after electrochemical experiments attributable to Mo-N groups originally present in the film. We therefore suggest that extra care should be taken during the electrode fabrication process to avoid incorporation of N impurities. As we have demonstrated, cathodic N leaching complicates analyses of ammonium ions in electrolytes. Moreover, a direct comparison of experiments under Ar/N_2 purging must be made before robustly establishing claims of electrochemical reduction of N_2 to NH_3. We note that another pre-reduction strategy has been used to remove N impurities in electrodes prior to N_2-reduction tests.[34]

Concluding Remarks

Extensive investigations employing $^{15}N_2$(g) as the potential reactant failed to confirm electrocatalytic activities of CoMo thin-film electrodes in aqueous and ethanolic H_2SO_4 for conversion of N_2 to NH_3. Simultaneous quantification of $^{14}NH_4^+/^{15}NH_4^+$ concentrations using a dansyl chloride derivatization/UPLC-MS method indicated that the increased ammonium concentrations observed after electrolyses were solely derived from $^{14}NH_4^+$ rather than $^{15}NH_4^+$. Based on these findings, we conclude that the additional ammonium ions originated from N impurities in CoMo thin-films, and that these

impurities entered the electrolyte when the electrode was under cathodic conditions.

Our findings are in accord with those based on definitive work in other laboratories,[20,35,36] hence we close with a few take-home lessons for the nitrogen fixation/reduction community (Table 3): (1) perform extensive control experiments for more precise ammonia quantification; (2) identify and remove all possible ammonia contamination sources, especially $^{15}NH_3$ impurities in $^{15}N_2$ gas (as identified in our study); (3) carefully monitor ammonium concentrations during each experimental step; and (4) perform electrolyses using both pure $^{15}N_2$ (with gas bubbler) and Ar gas; and compare ammonium yields under both conditions to evaluate electrode activities.

Table 3. Ammonia contamination sources

Ammonia contamination source	Recommended action
Ambient ammonia contamination	Extensive control experiments
Various electrochemical test components (electrolyte/RE/CE/EC cell/epoxy, etc.)	Careful sampling of electrolyte during each experiment step
NH_3 in N_2 gas (both $^{14}N/^{15}N$)	Use gas bubblers: confirm removal of NH_3 before/after purging
Plastic (polypropylene) analysis vials	Use glass vials; minimize sample storage time
N-based impurities in electrode materials	Compare results of N_2/Ar-purging experiments

Acknowledgments

K.B. acknowledges funding from the fellowship program of the German National Academy of Sciences - Leopoldina, grant LPDS 2016-06. Acknowledgment is made to the donors of The American Chemical Society Petroleum Research Fund for partial support of this research. Sample preparation and analyses were performed at the Joint Center for Artificial Photosynthesis, supported through the Office of Science of the U.S. Department of Energy under Award Number DE-SC0004993, which also provided support for N.S.L.. W.Y., P.B. and C.G.R. and K.B. acknowledge use of instrumentation in the Molecular Materials Research Center of the Beckman Institute at Caltech. N.F.D. is grateful to the Linde Center for support. The Environmental Analysis Center is supported by the Beckman Institute at Caltech. W.Y. and C.G.R. acknowledge the Resnick Sustainability Institute at Caltech for fellowship support. Dr. Fabai Wu and Prof. Victoria Orphan are acknowledged for providing the $^{15}NH_4Cl$ standard reagent for UPLC-MS analysis. Mr. Christopher Kenseth is thanked for assistance with UPLC-MS analysis. Dr. Yuanlong Huang is acknowledged for assistance with chemiluminescence analysis. All authors would like to acknowledge the reviewers for their valuable comments in the first round.

References

1 L. Wang, M. Xia, H. Wang, K. Huang, C. Qian, C. T. Maravelias and G. A. Ozin, *Joule*, 2018, **2**, 1055–1074.
2 A. R. Singh, B. A. Rohr, J. A. Schwalbe, M. Cargnello, K. Chan, T. F. Jaramillo, I. Chorkendorff and J. K. Nørskov, *ACS Catalysis*, 2017, **7**, 706–709.
3 J. S. Anderson, J. Rittle and J. C. Peters, *Nature*, 2013, **501**, 84–87.
4 M. J. Chalkley, T. J. Del Castillo, B. D. Matson and J. C. Peters, *Journal of the American Chemical Society*, 2018, **140**, 6122–6129.
5 C. J. M. van der Ham, M. T. M. Koper and D. G. H. Hetterscheid, *Chemical Society Reviews*, 2014, **43**, 5183–5191.

6 B. H. R. Suryanto, D. Wang, L. M. Azofra, M. Harb, L. Cavallo, R. Jalili, D. R. G. Mitchell, M. Chatti and D. R. MacFarlane, *ACS Energy Letters*, 2019, **4**, 430–435.
7 M. Wang, S. Liu, T. Qian, J. Liu, J. Zhou, H. Ji, J. Xiong, J. Zhong and C. Yan, *Nature Communications*, , DOI:10.1038/s41467-018-08120-x.
8 J. M. McEnaney, A. R. Singh, J. A. Schwalbe, J. Kibsgaard, J. C. Lin, M. Cargnello, T. F. Jaramillo and J. K. Nørskov, *Energy & Environmental Science*, 2017, **10**, 1621–1630.
9 A. R. Singh, B. A. Rohr, M. J. Statt, J. A. Schwalbe, M. Cargnello and J. K. Nørskov, *ACS Catalysis*, 2019, **9**, 8316–8324.
10 X. Xue, R. Chen, C. Yan, P. Zhao, Y. Hu, W. Zhang, S. Yang and Z. Jin, *Nano Research*, 2019, **12**, 1229–1249.
11 J. Deng, J. A. Iñiguez and C. Liu, *Joule*, 2018, **2**, 846–856.
12 C. J. H. Jacobsen, S. Dahl, B. S. Clausen, S. Bahn, A. Logadottir and J. K. Nørskov, *Journal of the American Chemical Society*, 2001, **123**, 8404–8405.
13 C. J. H. Jacobsen, *Chemical Communications*, 2000, 1057–1058.
14 R. Kojima and K. Aika, *Chemistry Letters*, 2000, **29**, 514–515.
15 C. D. Zeinalipour-Yazdi, J. S. J. Hargreaves and C. R. A. Catlow, *The Journal of Physical Chemistry C*, 2015, **119**, 28368–28376.
16 C. D. Zeinalipour-Yazdi, J. S. J. Hargreaves and C. R. A. Catlow, *The Journal of Physical Chemistry C*, 2018, **122**, 6078–6082.
17 I. J. McPherson, T. Sudmeier, J. Fellowes and S. C. E. Tsang, *Dalton Transactions*, 2019, **48**, 1562–1568.
18 J. G. Howalt and T. Vegge, *Physical Chemistry Chemical Physics*, 2013, **15**, 20957.
19 Y. Tsuji, K. Ogasawara, M. Kitano, K. Kishida, H. Abe, Y. Niwa, T. Yokoyama, M. Hara and H. Hosono, *Journal of Catalysis*, 2018, **364**, 31–39.
20 S. Z. Andersen, V. Čolić, S. Yang, J. A. Schwalbe, A. C. Nielander, J. M. McEnaney, K. Enemark-Rasmussen, J. G. Baker, A. R. Singh, B. A. Rohr, M. J. Statt, S. J. Blair, S. Mezzavilla, J. Kibsgaard, P. C. K. Vesborg, M. Cargnello, S. F. Bent, T. F. Jaramillo, I. E. L. Stephens, J. K. Nørskov and I. Chorkendorff, *Nature*, 2019, **570**, 504–508.
21 A. C. Nielander, J. M. McEnaney, J. A. Schwalbe, J. G. Baker, S. J. Blair, L. Wang, J. G. Pelton, S. Z. Andersen, K. Enemark-Rasmussen, V. Čolić, S. Yang, S. F. Bent, M. Cargnello, J. Kibsgaard, P. C. K. Vesborg, I. Chorkendorff and T. F. Jaramillo, *ACS Catalysis*, 2019, **9**, 5797–5802.
22 J. Kibsgaard, J. K. Nørskov and I. Chorkendorff, *ACS Energy Letters*, 2019, **4**, 2986–2988.
23 C. MacLaughlin, *ACS Energy Letters*, 2019, **4**, 1432–1436.
24 R. Y. Hodgetts, A. S. Kiryutin, P. Nichols, H.-L. Du, J. M. Bakker, D. R. Macfarlane and A. N. Simonov, *ACS Energy Letters*, 2020, 736–741.
25 W. T. Bolleter, C. J. Bushman and P. W. Tidwell, *Analytical Chemistry*, 1961, **33**, 592–594.
26 B. Cao, G. M. Veith, J. C. Neuefeind, R. R. Adzic and P. G. Khalifah, *Journal of the American Chemical Society*, 2013, **135**, 19186–19192.
27 S. Podila, S. F. Zaman, H. Driss, Y. A. Alhamed, A. A. Al-Zahrani and L. A. Petrov, *Catalysis Science & Technology*, 2016, **6**, 1496–1506.
28 X. Fu, H. Su, W. Yin, Y. Huang and X. Gu, *Catalysis Science & Technology*, 2017, **7**, 1671–1678.

29 W. Yu, N. S. Lewis, H. B. Gray and N. F. Dalleska, *ACS Energy Letters*, 2020, 1532–1536.
30 R. Dabundo, M. F. Lehmann, L. Treibergs, C. R. Tobias, M. A. Altabet, P. H. Moisander and J. Granger, *PLoS ONE*, 2014, **9**, e110335.
31 H.-L. Du, T. R. Gengenbach, R. Hodgetts, D. R. MacFarlane and A. N. Simonov, *ACS Sustainable Chemistry & Engineering*, 2019, **7**, 6839–6850.
32 B. Hu, M. Hu, L. Seefeldt and T. L. Liu, *ACS Energy Letters*, 2019, **4**, 1053–1054.
33 M. A. Shipman and M. D. Symes, *Catalysis Today*, 2017, **286**, 57–68.
34 H. Liu, Y. Zhang and J. Luo, *Journal of Energy Chemistry*, 2020, **49**, 51–58.
35 L. F. Greenlee, J. N. Renner and S. L. Foster, *ACS Catalysis*, 2018, **8**, 7820–7827.
36 B. H. R. Suryanto, H.-L. Du, D. Wang, J. Chen, A. N. Simonov and D. R. MacFarlane, *Nature Catalysis*, 2019, **2**, 290–296.